Protein synthesis inhibitors and the chemical chaperone TMAO reverse endoplasmic reticulum perturbation induced by overexpression of the iodide transporter pendrin

Jeanne Shepshelovich[1], Lee Goldstein-Magal[1], Anat Globerson[1], Paul M. Yen[2], Pnina Rotman-Pikielny[3] and Koret Hirschberg[1,*]

[1]Department of Pathology, Sackler School of Medicine, Tel-Aviv University, Tel-Aviv 69978, Israel
[2]Johns Hopkins Bay View Medical Center, Johns Hopkins University, Baltimore, MD 21224, USA
[3]Department of Internal Medicine E, Meir Hospital Sapir Medical Center, Kfar-Sava, Israel
*Author for correspondence (e-mail: koty@post.tau.ac.il)

Accepted 28 January 2005
Journal of Cell Science 118, 1577-1586 Published by The Company of Biologists 2005
doi:10.1242/jcs.02294

Summary

An outcome of overloading of the endoplasmic reticulum (ER) folding machinery is a perturbation in ER function and the formation of intracellular aggregates. The latter is a key pathogenic factor in numerous diseases known as ER storage diseases. Here, we report that heterologous overexpression of the green fluorescent protein-tagged iodide transporter pendrin (GFP-PDS) perturbs folding and degradation processes in the ER. Pendrin (PDS) is a chloride-iodide transporter found in thyroid cells. Mutations in PDS can cause its retention in the ER and are associated with Pendred syndrome. Biochemical and live-cell analyses demonstrated that wild-type GFP-PDS is predominantly retained in perinuclear aggregates and in ER membranes, causing their collapse and vesiculation. Inhibition of protein synthesis by cycloheximide (CHX) or puromycin caused dissociation of the GFP-PDS aggregates and returned the ER to its normal reticular morphology. Blocking protein synthesis promoted folding and export of ER-retained GFP-PDS, as demonstrated by surface-biotinylation analysis and by CHX- or puromycin-induced accumulation of YFP-PDS in the Golgi apparatus during a 20°C temperature-block experiment. The chemical chaperone trimethylamine-*N*-oxide (TMAO) also reversed the GFP-PDS-mediated ER collapse and vesiculation, suggesting that exposed hydrophobic stretches of misfolded or aggregated GFP-PDS may contribute to ER retention. These data suggest that GFP-PDS is a slow-folding protein with a propensity to form aggregates when overexpressed. Thus, we describe a system for the reversible induction of ER stress that is based entirely on the heterologous overexpression of GFP-PDS.

Supplementary material available online at
http://jcs.biologists.org/cgi/content/full/118/8/1577/DC1

Key words: Pendrin, Green fluorescent protein, Endoplasmic reticulum, Aggregation, Folding, ERAD

Introduction

Newly synthesized transmembrane proteins are co-translationally inserted into ER membranes, where the ER folding machinery catalyzes the proper folding necessary for normal function (Ellgaard and Helenius, 2003). Many proteins are rapidly and efficiently processed, pass the ER quality-control system and proceed through the secretory pathway. However, a growing number of improperly folded proteins that cannot pass the ER's stringent quality control are being discovered (Cobbold et al., 2003). Incompletely folded membrane proteins are eliminated by the ER-associated degradation (ERAD) system, which is initiated by ubiquitilation and followed by retro-translocation and proteasomal degradation in the cytosol (Hampton, 2002). Perturbation of proteasomal degradation results in the formation of intracellular protein aggregates (Johnston et al., 1998). The occurrence of intra- and extracellular protein aggregates in many degenerative diseases emphasizes the physiological importance of ER quality-control pathways. Failure of these systems to either avoid or deal with aggregate formation has detrimental consequences for cells and organisms. Aggregated proteins are delivered specifically to the perinuclear region on microtubular tracks by dynein-dependent transport. This microtubule-dependent inclusion body is called an aggresome. The unfolded protein response is a well-characterized, multifaceted signaling pathway aimed at avoiding the formation of protein aggregates. However, the mechanisms utilized by cells to deal with proteins once they have aggregated are mostly unknown. It has been postulated that the cellular machinery directs aggregated proteins into perinuclear inclusion bodies as a means of protecting cells from multiple toxic protein aggregates.

One of the most studied examples of misfolded proteins is the cystic fibrosis transmembrane conductance regulator

(CFTR) (Kopito, 1999). Most synthesized CFTR molecules never reach a folded state and are retained in the ER to serve as substrates for ERAD (Ward and Kopito, 1994). According to the current hypothesis, proteins having minimal Gibbs-free-energy differences between their unfolded and folded states are trapped in the ER for extended periods and serve as substrates for repeated folding attempts, as well as for the ERAD system (Gazit, 2002; Helenius, 2001). A recent study has shown that inefficient processing of CFTR occurs only in heterologous overexpression systems. In epithelial cells, endogenously expressed CFTR is efficiently processed and exported to post-Golgi compartments (Varga et al., 2004).

In this study, we examined the relationship between the intracellular distribution and ER processing of pendrin (PDS), a plasma membrane (PM) iodide transporter. The *Pendred* gene is a member of the SLC26 gene family (SLC26A4). The gene product, PDS, is a 780 amino acid, 73 kDa membrane glycoprotein, containing 12 putative transmembrane domains and three *N*-glycosylation sites (Everett et al., 1997). PDS, a key protein in the metabolic pathway of iodide, resides in the apical domain of thyroid follicular cells (Gillam et al., 2004; Scott et al., 1999). Mutations in PDS cause Pendred syndrome, an autosomal recessive disorder characterized by congenital deafness, goiter and defective iodide organification. The mechanism of the disease has been shown to involve retention in the ER, at least for the three mutations L236P, T416P and G384E. This was demonstrated by two independent studies using wild-type and mutant PDS tagged with green fluorescent protein (GFP) (Rotman-Pikielny et al., 2002; Taylor et al., 2002). It was stated that although wild-type GFP-PDS arrives at the PM, a significant population is observed intracellularly (Rotman-Pikielny et al., 2002; Taylor et al., 2002). In this study, we combined biochemical and live-cell analyses to examine the intracellular distribution of GFP-tagged wild-type PDS in a heterologous overexpression system. Although GFP-PDS is correctly targeted to the PM in a variety of cell lines (MDCK, CV1, COS7, NRK, CHO, HEK-293, FRTL-5), most of the protein is retained in the ER and in intracellular aggregates. Retention and accumulation in the ER cause its rapid and distinct morphological collapse, characterized by condensation and vesiculation of ER membranes around the nucleus, malformation of the nuclear envelope and formation of aggregates. However, blocking protein synthesis was sufficient to effectively reverse the ER's abnormal morphology and, at later stages, completely eliminate the ER pool of GFP-PDS. We demonstrate that upon inhibition of protein synthesis, ER-retained GFP-PDS is targeted to ERAD, as well as exported to the PM. Furthermore, in the presence of the naturally occurring chemical chaperone trimethylamine-*N*-oxide (TMAO) (Zou et al., 2002), the vesiculated morphology of the ER is reversed, indicating that it is induced by the accumulation of exposed hydrophobic peptide stretches of misfolded GFP-PDS. Thus, we demonstrate that heterologous overexpression of GFP-PDS is a powerful model system for the induction of reversible ER stress without the need for pharmaceutical agents.

Materials and Methods

Reagents and constructs

The proteasome inhibitor N-carbobenzoxyl-Leu-Leu-Leucinal (ALLN) was purchased from ICN (Irvine, CA). All other reagents, including the protein-synthesis inhibitors cycloheximide (CHX), puromycin and trimethylamine-*N*-oxide (TMAO), were purchased from Sigma Chemical Co. (St Louis, MO). GFP, CFP or YFP-PDS and GFP, CFP or YFP-L236P were generated as described (Rotman-Pikielny et al., 2002). Briefly, PDS cDNA was subcloned into various GFP expression vectors, pEGFP-C1, pECFP-C1 or pEYFP-C1 (Clontech, Palo Alto, CA), using *Xho*I and *Kpn*I restriction sites. Free PDS was subcloned from GFP-PDS into pCDNA4B (Invitrogen, Paisley, UK) using *Xho*I and *Sac*II. Mutations were created using the QuickChange™ Site-Directed Mutagenesis Kit (Stratagene, La Jolla, CA) according to manufacturer's directions. GPI-YFP, VSVGtsO45-YFP and sec61β-YFP were prepared as described elsewhere (Nichols et al., 2001; Snapp et al., 2003; Ward et al., 2001). GFP-CFTR was a kind gift from B. Stanton (Dartmouth Medical School, Hanover, NH). The red fluorescent protein diHcRED was a kind gift from Jan Ellenberg (EMBL, Heidelberg, Germany).

Cell culture and transfection

COS7 (African green monkey kidney) cells were grown at 37°C in a humidified atmosphere with 5% CO_2. Cell cultures were maintained in Dulbecco's modified Eagle's medium (DMEM) supplemented with 10% (v/v) fetal bovine serum (FBS) and penicillin/streptomycin (Biological Industries, Bet-Haemek, Israel). For microscopy, cells were sub-cultured in Labtek glass coverslip chambers (Nalgene Nunc International, Rochester, NY). Cells were grown to between 50 and 60% confluence and then transfected with 0.5-1.5 μg DNA per Labtek chamber (8.4 cm^2) using FuGENE-6 reagent (Roche Applied Science, Mannheim, Germany). Experiments and confocal laser-scanning microscopy images were obtained from 16 to 18 hours after transfection.

Immunofluorescence microscopy

Cells grown on glass coverslips were fixed in a 2% (v/v) formaldehyde solution. After three washes, the primary antibodies, anti-PDS rabbit polyclonal h630-643 or anti-ubiquitin (monoclonal P4D1; Santa Cruz Biotechnology, Santa Cruz, CA) and Cy3 secondary antibodies diluted in PBS containing 5% FBS and 0.2% (v/v) saponin were applied for 1 hour at 37°C. Coverslips were mounted for confocal image analysis.

Confocal laser-scanning microscopy and live-cell imaging

Cells were imaged in DMEM without phenol red but supplemented with 20 mM Hepes, pH 7.4, as already described. Transfection and imaging were performed in the Labtek chambers. A Zeiss LSM PASCAL equipped with an Axiovert 200 inverted microscope and Ar 458 nm, 488 nm and 514 nm lasers was used for ECFP, EGFP and EYFP. A HeNe 543 nm laser was used for Cy3. The confocal images were captured using a 63× 1.4 NA objective with a pinhole diameter equivalent to between 1 and 2 Airy units. Time-lapse images were captured with a 25× 0.8 NA objective. Image capture was carried out using the advanced multi-time series macro set, with embedded reflection-mode autofocusing (Zeiss, Jena, Germany), in the presence of an electronic temperature-controlled air-stream incubator. Images and movies were generated and analyzed using the Zeiss LSM software and NIH Image software (W. Rasband, NIH, Bethesda, MD).

Western blot analysis and immunoprecipitation

COS7 cells expressing GFP-PDS or GFP-L236P were scraped into lysis buffer containing 1% (v/v) Triton X-100 and protease inhibitor cocktail (Roche). The cell lysate was centrifuged in a Sigma centrifuge for 30 minutes at 21,900 ***g***, 4°C. The supernatant was collected, protein concentrations were determined and samples of 15

μg protein were separated on a 6% SDS-polyacrylamide gel then transferred to a nitrocellulose membrane (BioRad Laboratories, Hertfordshire, UK). Membranes were blocked and probed for the expression of GFP (monoclonals 7.1+13.1; Roche), pendrin (rabbit polyclonal h630-643) or ubiquitin (monoclonal P4D1; Santa Cruz Biotechnology) antibodies. The secondary peroxidase-conjugated antibody was sheep anti-mouse IgG (NA 931; Amersham Pharmacia Biotech, Piscataway, NJ) or goat anti-rabbit IgG (BioRad). Detection was carried out using an enhanced chemiluminescence (ECL) SuperSignal kit (Pierce, Rockford, IL). As a loading control, membranes were cut and probed with monoclonal anti-β-actin antibody (Sigma). GFP-PDS was immunoprecipitated from cell extracts with anti-GFP antibody. Conjugates were incubated with protein G agarose beads (Sigma) overnight at 4°C on a rotator. Complexes were washed and used for western blot analysis.

Surface biotinylation

Prior to their extraction, cells were incubated on ice for 60 minutes with the membrane-impermeable reagent EZ-link™ sulfosuccinimidyl-6-(biotinamido)-hexanoate (Pierce). Biotinylated conjugates were affinity-purified with streptavidin agarose beads (Sigma) on a rotator for 3 hours at 4°C, separated by SDS-PAGE and detected on a western blot using anti-GFP antibody.

Protease protection assay

To test the amount of GFP-PDS aggregates, we extracted total cell lysates in lysis buffer without protease inhibitors. Trypsin (0.05% w/v; Biological Industries) was added for the indicated incubation times. The reaction was stopped by adding sample buffer. Digestion products were separated by SDS-PAGE and blotted as already described.

Results

Intracellular localization of GFP-PDS

ER retention of PDS mutants was previously demonstrated using GFP-tagged chimeras (Rotman-Pikielny et al., 2002; Taylor et al., 2002). To demonstrate the strong tendency of GFP-PDS to accumulate in ER membranes and form aggregates, we compared its intracellular distribution with that of GFP-CFTR, a well-studied case of a misfolding protein (Kopito, 1999). In Fig. 1A, the intracellular distributions of heterologously overexpressed wild-type PDS protein, GFP-PDS chimera and GFP-CFTR are compared. Confocal images of COS7 cells, either fixed for immunofluorescence with rabbit anti-PDS and secondary Cy3 anti-rabbit antibodies, or live, expressing GFP-PDS or GFP-CFTR, are shown. Clear labeling of the PM demonstrates that both untagged PDS and GFP-PDS arrive there. However, most of the protein is localized intracellularly, in the ER membranes (Fig. 1A; Fig. S1 in supplementary material) and in perinuclear aggregates, the latter failing to recover after photobleaching (Fig. 1B). Interestingly, the slow-folding GFP-CFTR, under identical conditions of expression, is efficiently targeted to the PM with no apparent accumulation in the ER.

To confirm and quantify the localization of GFP-PDS in the PM, we used surface-biotinylation analysis. Cells expressing GFP-PDS or its GFP-tagged mutant, L236P (GFP-L236P), which has been previously shown to be retained in the ER (Rotman-Pikielny et al., 2002), were subjected to surface biotinylation. Cells were then lysed and analyzed by western blotting. There were no detectable levels of biotinylated GFP-L236P, whereas 4% of the total (soluble and insoluble) GFP-PDS localized to the PM (Fig. 1C). In addition, 9% of the GFP-PDS and 23% of the GFP-L236P were insoluble and thus sedimented in the low-speed pellet (14 K). This insoluble fraction may correspond to the GFP-PDS in perinuclear aggregates.

Next, we assessed the effect of overexpression of GFP-PDS on the ER's degradation and folding functions. The total cellular ubiquitilation profile was examined in cells expressing GFP-PDS, GFP-L236P, GFP-CFTR or the GFP-tagged, ER-retained Δ508 CFTR mutant (GFP-ΔF508), by western blot with anti-ubiquitin antibody (Fig. 1D). The ubiquitilated proteins accumulated exclusively in cells expressing GFP-PDS or GFP-L236P, indicating inhibition of ERAD. To further examine the effect of GFP-PDS overexpression on the ER's folding function, we analyzed the effect of GFP-PDS on the processing of a misfolded protein accumulated there. The tsO45 thermo-reversible folding mutant of vesicular stomatitis virus G protein, tagged with GFP (GFP-VSVG), was overexpressed in COS7 cells with or without GFP-PDS. At the non-permissive temperature (40°C), GFP-VSVG is reversibly misfolded and accumulates within ER membranes. Upon temperature shift to the permissive temperature (32°C), it refolds and is rapidly transported to the PM (Presley et al., 1997). The level of PM-localized GFP-VSVG detected by surface biotinylation was much lower in cells co-expressing GFP-PDS and GFP-VSVG than in control cells expressing only GFP-VSVG (Fig. 1E). These data indicate that both ERAD and the folding function of the ER are affected by overexpression of GFP-PDS.

GFP-PDS accumulation causes vesiculation of ER membranes

An apparent morphological consequence of GFP-PDS and PDS overexpression is the transformation of ER membranes from a reticular to a dilated vesicular structure (see Fig. S1 in supplementary material for untagged PDS). To demonstrate the transformation of the ER's membrane topology from reticular to dense dilated vesicular structure, COS7 cells were co-transfected with YFP-PDS and either cytosolic, free CFP or CFP containing the cleavable signal sequence of hen-egg-lysosyme (helss-CFP), an ER luminal marker. The scheme on the right in Fig. 2 summarizes the intracellular localization of the cytosolic and ER-luminal CFP markers relative to YFP-PDS. In Fig. 2A, the cytosolic CFP can be seen localized to the cytosol and cell nucleus, and excluded from the inner luminal space of the vesicles. The localization of helss-CFP within the lumen of the vesicular structures confirms that they are ER membranes (Fig. 2B).

The effect of inhibition of protein synthesis on the intracellular processing and distribution of GFP-PDS

GFP-PDS effectively perturbs ER function. This effect is accompanied by a distinct morphological transformation of ER membranes as well as the formation of perinuclear GFP-PDS aggregates. We were interested in determining whether these extreme effects could be reversed or if subsequent cell death was inevitable. To assess the reversibility of the effects induced by overexpression of GFP-PDS, we examined the effects of inhibition of protein synthesis on the intracellular processing

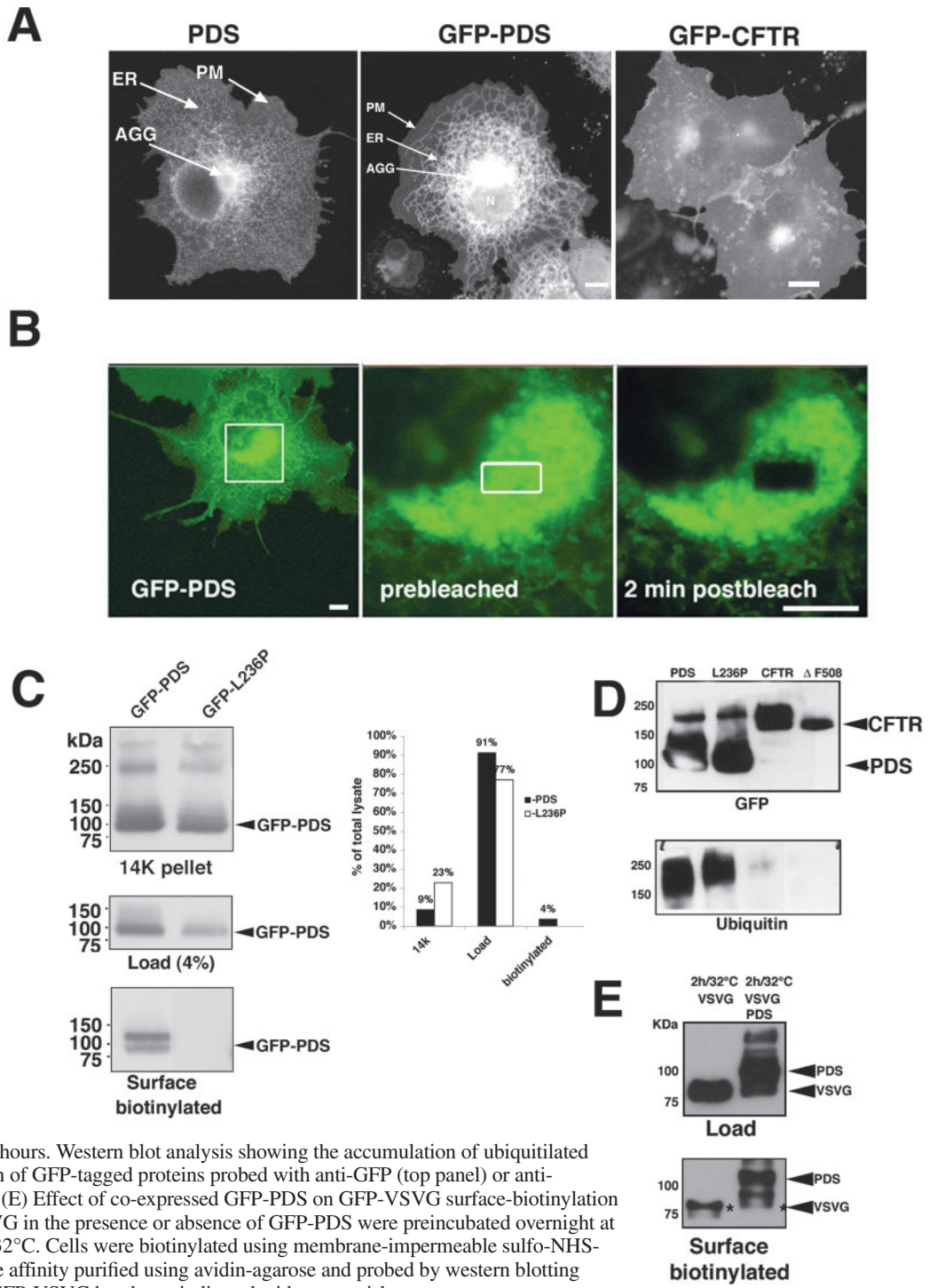

Fig. 1. Intracellular distribution of GFP-PDS and effect on ER function in COS7 cells. (A) Confocal images of fixed cells expressing untagged PDS, and living cells expressing GFP-PDS and GFP-CFTR, 16 hours after transfection. Cells expressing untagged PDS were fixed, permeabilized and probed with anti-PDS antibody and secondary Cy3 anti-rabbit antibody as described in Materials and Methods. GFP and Cy3 were detected with Ar 488 nm and HeNe 543 nm laser lines, respectively. Arrows indicate the plasma membrane (PM), endoplasmic reticulum (ER) and perinuclear aggregate (AGG). Bars, 10 μm. (B) Perinuclear GFP-PDS forms aggregates as demonstrated by photobleaching. A rectangle in the middle of a perinuclear aggregate was photobleached in a cell expressing GFP-PDS using a high-power 488 nm laser. Bars, 10 μm. (C) Detection of surface GFP-PDS and GFP-L236P by biotinylation. Cells were biotinylated using membrane-impermeable sulfo-NHS-biotin. Surface-labeled proteins were affinity purified using avidin-agarose and probed by western blotting using anti-GFP mAb. Results of quantitative densitometry are presented, on the right, as percentage of the sum of total lysate and low speed (14K) pellet. (D) Western blot analysis of the effect of GFP-PDS, GFP-L236P, GFP-CFTR and GFP-Δ508 expression on proteasomal degradation. Cells were transfected with equal amounts of plasmids as described in Materials and Methods and harvested after 16 hours. Western blot analysis showing the accumulation of ubiquitilated proteins as a result of overexpression of GFP-tagged proteins probed with anti-GFP (top panel) or anti-ubiquitin (bottom panel) antibodies. (E) Effect of co-expressed GFP-PDS on GFP-VSVG surface-biotinylation labeling. Cells expressing GFP-VSVG in the presence or absence of GFP-PDS were preincubated overnight at 40°C prior to 2 hours incubation at 32°C. Cells were biotinylated using membrane-impermeable sulfo-NHS-biotin. Surface-labeled proteins were affinity purified using avidin-agarose and probed by western blotting using anti-GFP mAb. Biotinylated GFP-VSVG bands are indicated with an asterisk.

and distribution of GFP-PDS in live cells. We hypothesized that blocking the influx of nascent peptides (Novoa et al., 2003) would reduce the protein load on the ER processing and folding machineries. This was expected to allow a reversal of the effects generated by overexpressed GFP-PDS. To inhibit protein synthesis, we used the translation-elongation and translation-initiation inhibitors, CHX and puromycin, respectively. To visualize changes in cell morphology and in the intracellular distribution of GFP-PDS, as well as to confirm that the turnover and dissociation of GFP-PDS aggregates are facilitated by inhibition of protein synthesis, we used live-cell microscopy. Live COS7 cells expressing GFP-PDS were continuously followed for 5 hours using a confocal laser-scanning microscope in the presence of 25 μg/ml CHX (a concentration found, by western blot analysis, to efficiently inhibit synthesis; data not shown). CHX-mediated turnover of GFP-PDS resulted in a complete reversal of the adverse morphological effects of GFP-PDS overexpression (Fig. 3A;

see also Movie 1 in supplementary material). The ER reverted to its normal reticular morphology and the intracellular levels of GFP-PDS decreased significantly. This is also demonstrated by the time-dependent decrease in fluorescence intensities in three regions of interest surrounding representative cells. Longer incubations with CHX or puromycin resulted in the exclusive localization of GFP-PDS to the PM, suggesting that its intracellular pool had been completely processed (Fig. 3B). Thus, the functional and morphological manifestations of ER stress induced by overexpression of GFP-PDS are completely reversible by blocking protein synthesis.

The effects of increasing concentrations of CHX on GFP-PDS solubility and turnover are shown in Fig. 3C. Cells expressing GFP-PDS were incubated for 6 h with increasing

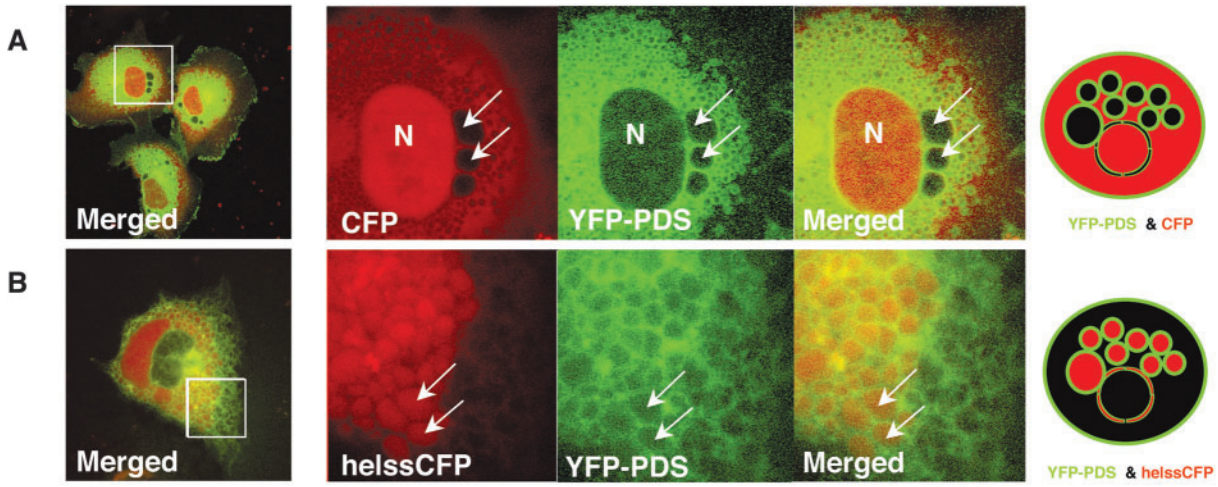

Fig. 2. Effect of GFP-PDS overexpression on ER morphology in COS7 cells. (A) Confocal images of cells co-expressing YFP-PDS and free cytosolic CFP. The ER is vesiculated and CFP (red) is excluded from the lumen of the vesicular membranes (white arrows). (B) Confocal images of cells co-expressing YFP-PDS and ER-luminal helss-CFP. The lumen of the vesicular membrane structures is labeled with helss-CFP, confirming that they are ER membranes. The relative topology and distributions of YFP-PDS (green) and CFP or helss-CFP (red) in each panel are summarized in the scheme on the right side.

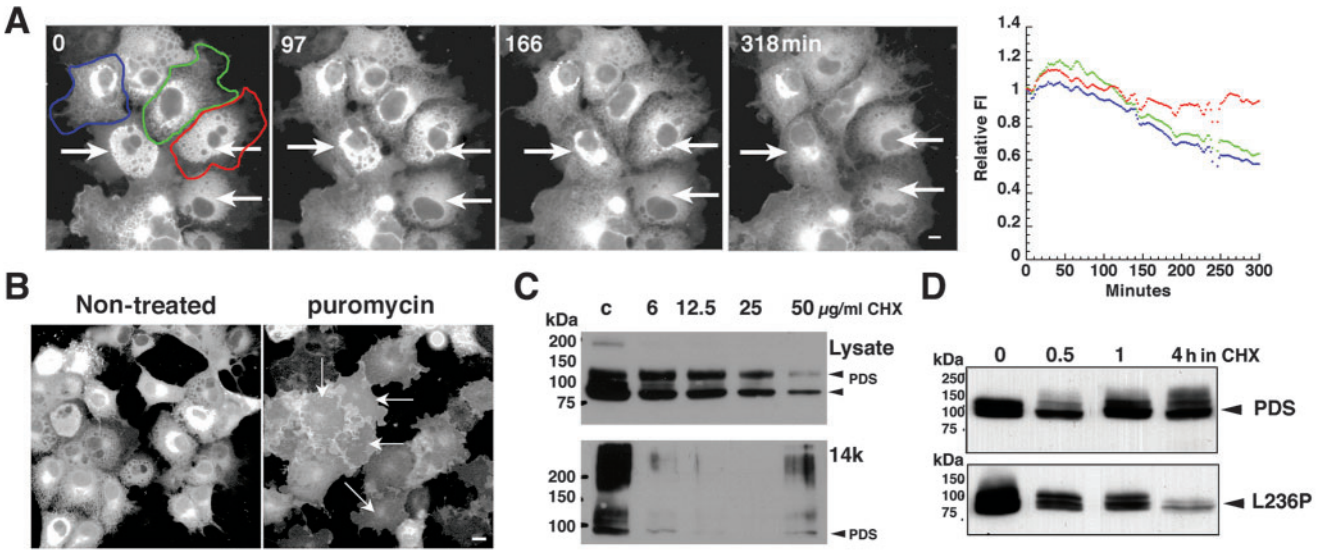

Fig. 3. Effect of inhibition of protein synthesis on solubility and intracellular distribution of GFP-PDS. (A) Live-cell analysis of CHX-mediated recovery of GFP-PDS-expressing cells. Representative images of a time-lapse sequence of cells expressing GFP-PDS incubated in the presence of 25 μg/ml CHX for 5.3 hours. Images were captured at 45-second intervals. Arrows indicate cells with recovering ER. Right: regions of interest of total cellular fluorescence are plotted against time for the three cells outlined in the 0 minute panel. Bars, 20 μm. See also Movie 1 in supplementary material. (B) Live-cell microscopy of puromycin-mediated redistribution of the ER-retained GFP-PDS. Confocal images of cells expressing GFP-PDS incubated for 6 hours with or without 160 μg/ml puromycin. Bars, 10 μm. (C) Western blot analysis of the effect of CHX on GFP-PDS solubilization and degradation. Cells expressing GFP-PDS were incubated with increasing concentrations of CHX for 6 hours. Cell lysates (15 μg protein, top panel) and the 14K pellet (total pellet loaded, bottom panel) were probed with anti-PDS antibodies. (D) CHX-mediated degradation of GFP-PDS and GFP-L236P by western blot. Cells expressing GFP-PDS or GFP-L236P were incubated for the designated times with 25 μg/ml CHX. Cell lysates (15 μg protein) were probed with anti-PDS antibodies.

concentrations of CHX. Western blot analysis of total lysates indicated that the level of GFP-PDS is inversely proportional to CHX concentration. However, the insoluble fraction of GFP-PDS was already mostly eliminated at a low concentration of CHX (6 μg/ml). The turnover of GFP-PDS and of the ER-retained, most common naturally occurring mutation GFP-L236P was compared by western blot analysis. GFP-PDS turnover was less efficient than the degradation of GFP-L236P (Fig. 3D). GFP-PDS degradation occasionally involved the appearance of various higher-molecular mass bands recognized by either anti-GFP or anti-PDS antibodies. We excluded the possibility that these bands result from N-glycan processing, since they were detected in cells treated with CHX and swainsonine (Goss et al., 1995), an inhibitor of *N*-glycan-processing in the Golgi apparatus (data not shown).

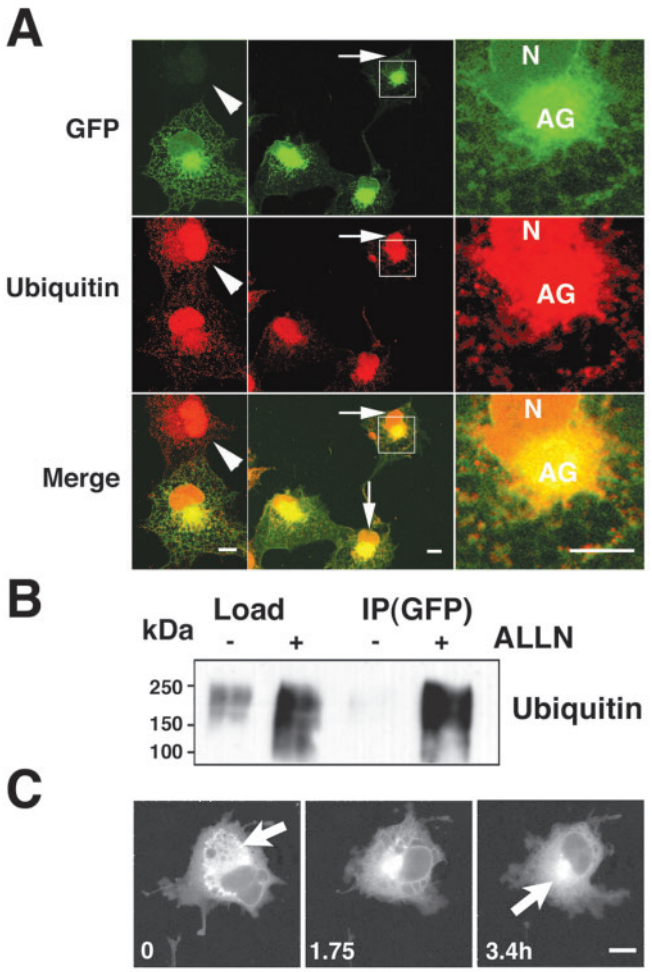

Fig. 4. GFP-PDS is ubiquitilated. (A) Immunofluorescence co-localization of GFP-PDS with ubiquitin. Confocal images of cells expressing GFP-PDS were treated with ALLN for 6 hours. Cells were fixed, permeabilized and probed with anti-ubiquitin mAb and secondary anti-mouse Cy3-tagged mAb. GFP and Cy3 were detected with Ar 488 nm and HeNe 543 nm laser lines, respectively. Magnified views on the left show aggregates of ubiquitilated (CK SP) GFP-PDS. Arrowheads in the left panels point to a non-GFP-PDS-expressing cell. Arrows indicate the nucleus. Boxed regions in the center panels are magnified fivefold to show perinuclear aggregates. N, nucleus; AG, aggregate. Bar, 20 μm. (B) Western blot analysis showing ubiquitilation of GFP-PDS by immunoprecipitation. Cells expressing GFP-PDS were incubated for 1 hour with ALLN. Anti-GFP mAb-GFP-PDS complexes were immunoisolated (IP) from lysates using protein G agarose and probed with anti-ubiquitin mAb. (C) Live-cell microscopy of CHX-mediated recovery of GFP-PDS-expressing cells in the presence of ALLN. Representative images from a time-lapse series of cells expressing GFP-PDS, incubated in the presence of 25 μg/ml CHX and 20 μg/ml ALLN for 3.5 hours. Images were captured at 45-second intervals. Arrows indicate GFP-PDS in aggregates and in collapsed ER. Bar, 20 μm. See also Movie 2 in supplementary material.

GFP-PDS is ubiquitilated

To confirm PDS as a substrate of the ubiquitin-proteasome pathway, immunofluorescence (Fig. 4A) and immunoprecipitation (Fig. 4B) analyses were carried out. The confocal images in Fig. 4A show that ubiquitin localizes primarily in the nucleus of cells that do not express GFP-PDS (Fig. 4A, left panel). In contrast, in cells expressing GFP-PDS, ubiquitin co-localizes specifically in the perinuclear region containing bright GFP-PDS or GFP-L236P (data not shown) aggregates. Immunoprecipitation of GFP-PDS with anti-GFP antibodies and western blot analysis with anti-ubiquitin antibodies, in the presence or absence of ALLN, also confirmed GFP-PDS ubiquitilation (Fig. 4B).

Next, we assessed whether the proteasome inhibitor ALLN affected the CHX-mediated reversal of the GFP-PDS overexpression phenotype (Fig. 4C). In the presence of ALLN and CHX, there was a significant improvement in cell morphology (Fig. 4C). GFP-PDS in the collapsed ER concentrated initially in small peripheral aggregates, which were then delivered to the perinuclear region. During this time, the ER membrane regained some of its reticular morphology (see Movie 2 in supplementary material). These data suggest that GFP-PDS is degraded by the proteasome, and that perinuclear GFP-PDS aggregates are ubiquitilated. In addition, the formation of perinuclear aggregates is suggested to be an intermediary stage in the CHX-mediated turnover of ER-retained GFP-PDS.

Effect of inhibition of protein synthesis on the folding and export of GFP-PDS

To test the hypothesis that inhibition of protein synthesis also helps to restore the function of the folding machinery, we examined the effect of CHX or puromycin on the folding and export of GFP-PDS. To demonstrate that GFP-PDS export from the ER is enhanced during inhibition of protein synthesis, we used surface-biotinylation labeling to analyze changes in the surface expression of GFP-PDS (Fig. 5A) and a 20°C temperature block to trap exported GFP-PDS in the Golgi apparatus (Fig. 5B). Fig. 5A shows the western blot analysis of surface-biotinylated cells preincubated with 450 mM sucrose and CHX or puromycin for 1 hour (Shefler and Sagi-Eisenberg, 2002). In the absence of 450 mM sucrose, PM-localized (biotinylated) GFP-PDS levels decreased during inhibition of synthesis, presumably because of internalization and degradation (Fig. S5 in supplementary material). CHX and puromycin facilitated the folding, and thus the surface expression, of GFP-PDS (Fig. 5A). The 20°C temperature block experiment (Fig. 5B) also demonstrated that YFP-PDS

molecules accumulate and co-localize with GalT-CFP in the Golgi complex only in cells incubated with the protein synthesis inhibitors. Thus a significant population of ER-retained GFP-PDS is successfully folded and exported to the PM in the presence of protein synthesis inhibitors.

TMAO promotes the dissociation of aggregated GFP-PDS and reverses vesiculated ER morphology

The major intracellular pools of GFP-PDS are in perinuclear aggregates and in the ER membranes that are eventually transformed as described in Fig. 2. The mechanism of ER vesiculation is unknown. The reversal of ER morphology is facilitated by the addition of CHX (Fig. 3A), indicating that the ER's vesiculate morphology is directly related to the accumulation of misfolded GFP-PDS. Thus, we hypothesized that proliferation of misfolded GFP-PDS within the ER membranes directly interferes with the machinery that maintains ER organization, leading to vesiculation. To test this hypothesis, namely that the proliferation of exposed hydrophobic peptides from partially folded GFP-PDS triggers ER vesiculation, we analyzed the effect of incubating cells overexpressing GFP-PDS with the chemical chaperone TMAO. This naturally occurring chemical chaperone prevents protein aggregation by binding to and masking the exposed hydrophobic peptides. The soluble fraction of GFP-PDS in whole-cell lysates increased in the presence of TMAO (Fig. 6A). Furthermore, TMAO, and to a lesser extent CHX, significantly reduced the resistance of GFP-PDS to protease digestion in whole-cell lysates. Given that TMAO has no direct effect on protein synthesis, we suggest that masking of the hydrophobic peptides shifted cellular GFP-PDS from an aggregated protease-resistant form to a soluble, protease-sensitive one. To assess whether TMAO activity on GFP-PDS solubilization affects ER morphology, digital images of live cells expressing GFP-PDS were captured at 30-second intervals for 1.5 hours in the presence of TMAO (see Movie 3 in supplementary material). Representative images in Fig. 6C demonstrate that within 35 to 40 minutes, ER morphology changed from vesicular to reticular. These data confirm that ER vesiculation results from the proliferation of exposed hydrophobic peptides of misfolded GFP-PDS.

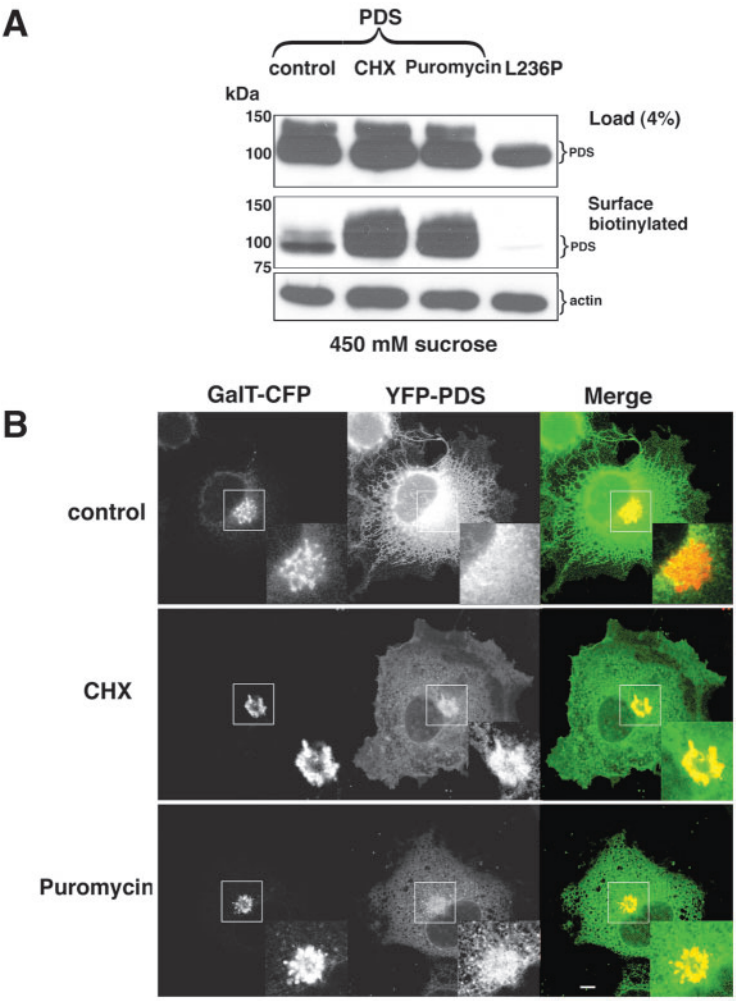

Fig. 5. Effect of inhibition of protein synthesis on folding and export of GFP-PDS. (A) Detection of CHX- and puromycin-mediated surface expression of GFP-PDS by biotinylation. Cells expressing GFP-PDS were incubated for 1 hour in culture medium containing 450 mM sucrose and 25 μg/ml CHX or 160 μg/ml puromycin. Cells were biotinylated using membrane-impermeable sulfo-NHS-biotin. Surface-labeled proteins were affinity-purified using avidin-agarose and probed by western blotting using anti-GFP and anti-actin mAbs as a loading control. (B) Confocal image analysis of CHX- or puromycin-mediated accumulation of YFP-PDS in the Golgi apparatus using a 20°C temperature block. Cells co-expressing YFP-PDS and the Golgi marker GalT-CFP were fixed after being incubated for 4 hours at 20°C in the presence of CHX or puromycin. Enlarged inserts show the perinuclear Golgi region. CFP- and YFP-tagged proteins were detected with Ar 458 nm and 514 nm laser lines, respectively. Bars, 10 μm.

In summary, we used live-cell imaging and biochemical analyses to examine the ER perturbations induced during less than 18 hours of GFP-tagged SLC26A4 iodide transporter overexpression in a heterologous system. Although GFP-PDS was correctly targeted to the PM, its overexpression disrupted the ER folding and degradation machineries, resulting in its accumulation in the ER and the formation of perinuclear aggregates. We show that inhibition of protein synthesis using CHX or puromycin can efficiently reverse these effects by facilitating the degradation and folding of GFP-PDS in the ER. Finally, by reversing the adverse effects of GFP-PDS on ER morphology, the naturally occurring chemical chaperone TMAO demonstrated that ER organization is interrupted by the exposed hydrophobic peptides of misfolded GFP-PDS.

Discussion

The final destination of correctly folded GFP-PDS is the PM. However, in heterologous expression systems (see Figs S1, S2, S3 in supplementary material), including stable expression, most of the protein is retained, accumulates and aggregates in the ER. GFP-PDS has been previously shown to be targeted to the PM and also localized intracellularly (Rotman-Pikielny et al., 2002; Taylor et al., 2002). In this study, surface-

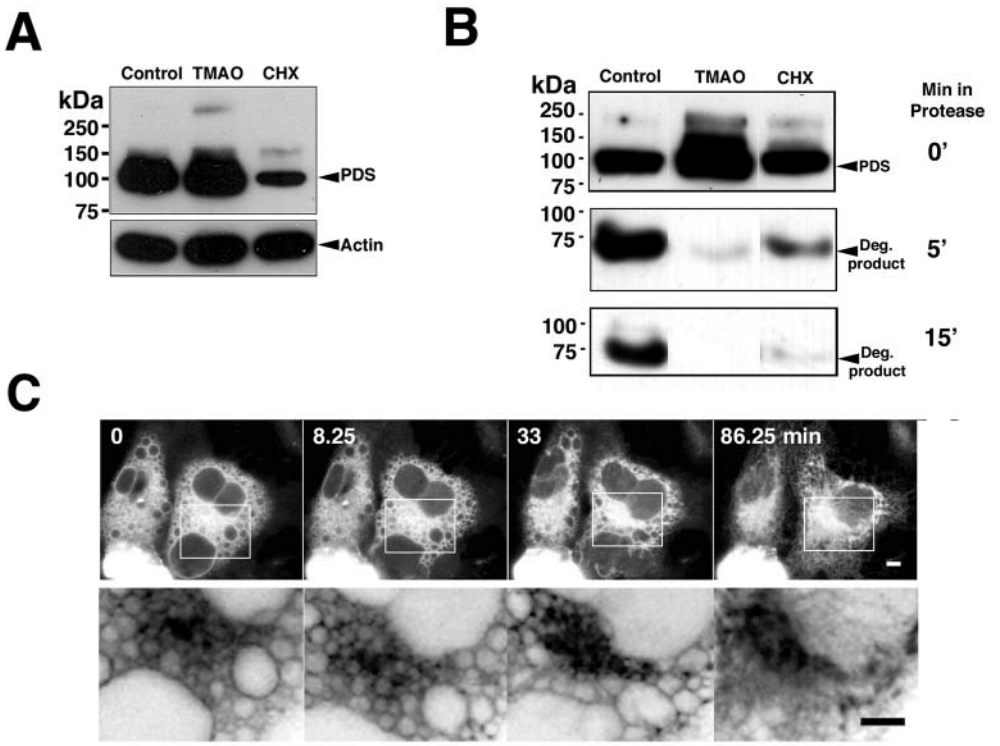

Fig. 6. Effect of TMAO on GFP-PDS aggregates and on ER morphology. (A) Western blot analysis of the effect of TMAO on GFP-PDS and GFP-L236P turnover. Cells expressing GFP-PDS were incubated with CHX or TMAO for 1 hour. Cell lysates (15 μg) were probed with anti-PDS antibodies and anti-actin mAbs as a loading control. (B) Protease protection assay of TMAO- and CHX-mediated GFP-PDS aggregate dissociation. Cells expressing GFP-PDS were incubated with CHX or TMAO for 1 hour. Cell lysates were incubated with protease for 5 and 15 minutes and probed with anti-GFP mAb by western blotting. (C) Analysis of TMAO-mediated ER recovery using live-cell microscopy. Confocal images of cells expressing GFP-PDS were captured at 45-second intervals for 3 hours after the addition of 150 mM TMAO. Bar, 10 μm. See also Movie 3 in supplementary material.

biotinylation analysis demonstrated that most (over 95%) of the GFP-PDS overexpressed in COS7 cells is retained intracellularly.

GFP-PDS accumulation in the ER probably results from its inefficient folding, which is a common feature of many polytopic proteins when overexpressed in heterologous systems (Varga et al., 2004). To examine the intracellular distribution of GFP-PDS at lower expression levels, we analyzed stable expression of GFP-PDS in normal rat kidney (NRK) cells, grown under selection of 500 μg/ml G418. The level of GFP-PDS expression in these cells was much lower than in COS7 cells, as determined by western blot analysis. However, confocal image analysis indicated that GFP-PDS accumulation in the ER is comparable with that in the transiently transfected cells (Figs S2 and S3 in supplementary material). Similar results were obtained when decreased levels of plasmid DNA were used in the transient transfection protocols for COS7 cells: GFP-PDS was undetectable by western blot analysis, with only a moderate effect on its intracellular distribution, based on fluorescence microscopy analysis (Fig. S2 in supplementary material).

The data in Fig. 1 suggests that GFP-PDS is an aggregate-forming, inefficiently folded protein, which tends to interfere with and saturate the folding and degradation functions of the ER (Johnston et al., 1998). Accumulation of ubiquitilated proteins in cells expressing GFP-PDS (Fig. 4) and GFP-L236P (data not shown) suggests that ERAD is perturbed. In comparison, overexpression of the slow-folding GFP-CFTR or its mutant GFP-Δ508, known substrates for ERAD, as well as folding in COS7 cells (Ward and Kopito, 1994), did not induce the accumulation of ubiquitilated proteins. Moreover, the low level of GFP-Δ508 is indicative of its normal rapid turnover in the ER. Thus, based on the results in Fig. 1, GFP-PDS more effectively perturbs ER function than GFP-CFTR.

Blocking of protein synthesis reverses the ER's loss of function and morphological transformation (Fig. 3). Three major processes are facilitated: dissociation of the aggregates, and degradation and folding of the ER-retained GFP-PDS. The efficient and rapid, but nevertheless, reversible perturbation of the ER, reached within less than 20 hours of transfection in the absence of pharmaceutical agents that typically have irreversible effects, constitutes a potentially powerful system to investigate the processes of aggregate dissociation as well as the outcome of unfolded protein response activation. Thus, this experimental system might prove to be important for understanding the mechanisms underlying 'protein deposition' and related neurodegenerative diseases (Kopito, 2000).

The live-cell analysis in Fig. 3A, and particularly Fig. 4C, in which protein synthesis was blocked while using the proteasome inhibitor ALLN, demonstrated that the formation of perinuclear aggregates is associated with the recovery of ER morphology. In some cases, the small peripheral aggregates that appeared during ER recovery were eliminated without being transported to the perinuclear region. Perinuclear aggregate formation is usually associated with higher levels of expression and their dissociation proceeds at a slower rate.

The facilitated reversal of the GFP-PDS phenotype by inhibition of protein synthesis can be attributed to the fact that ER stress-response proteins were already present prior to the addition of the inhibitors. However, it is also possible that the radical reduction in protein load was sufficient for the ER machinery to efficiently process the aggregated, ER-retained GFP-PDS.

Based on the findings shown in Figs 3, 4 and 5, ER-retained GFP-PDS is a substrate of both the folding and ERAD machineries, whereas GFP-L236P is exclusively an ERAD substrate. The fact that GFP-PDS refolding competes with degradation can explain its significantly slower turnover

relative to that of GFP-L236P (Fig. 3D and data not shown, respectively).

The marked effects of inhibition of protein synthesis demonstrate the capacity of unfolded protein response to relieve ER stress, via the attenuation of translation under physiological conditions (Novoa et al., 2003). During inhibition of protein synthesis, normal ER membranes emerge and spread outwards from the perinuclear-condensed, vesiculated ER and the vesiculate morphology is reversed at an early stage as well (see Movie 1 in supplementary material).

In a western blot analysis, both anti-GFP and anti-PDS antibodies frequently recognized a band of approximately 250 kDa. This band disappeared during incubations with CHX or puromycin, and it may therefore correspond to ubiquitilated GFP-PDS oligomer released from an intracellular aggregate (Fig. 4B). In this study, we provide evidence that GFP-PDS aggregates are actively dissociated upon inhibition of protein synthesis, as reflected by the increase in GFP-PDS solubility, as seen in Fig. 3C and Fig. 6B and in the live-cell analysis in Fig. 3A. The localization, topology and nature of the GFP-PDS-containing aggregates are unknown. The observation that ER membranes seem to emerge from them as a result of inhibition of protein synthesis suggests that they are different from classical cytosolic aggresomes (Bence et al., 2001). However, the fact that GFP-PDS perinuclear aggregates are heavily ubiquitilated does not rule out their cytosolic localization.

A possible mechanism for perturbation of the ER processing machinery by GFP-PDS is excessive chaperone occupation by partially folded GFP-PDS molecules and incoming GFP-PDS nascent chains. This in turn, results in the collapse of the ER towards the microtubular organizing center (MTOC) and vesiculation of the ER membranes. The abundance of hydrophobic stretches within GFP-PDS may cause the protein/protein aggregation interactions (Mount and Romero, 2004). The hypothesis that the hydrophobic nature of partially folded GFP-PDS causes ER collapse and vesiculation is further supported by the ability of TMAO to rapidly reverse this morphological transformation without affecting biosynthesis. TMAO is a natural chemical chaperone found mainly in deep-sea animals (Yancey et al., 2002). It is suggested that TMAO prevents protein aggregation by binding to, and thus masking exposed hydrophobic peptides. We therefore propose that by masking hydrophobic peptide stretches of GFP-PDS, TMAO compensates for the lack of hydrophobic-peptide-binding chaperones such as BIP, calnexin and calreticulin. BIP has been shown to bind hydrophobic peptides of misfolded glycoproteins (Blond-Elguindi et al., 1993) and is also the key chaperone for which the level of use in the ER is the activating factor of the unfolded protein response (Bertolotti et al., 2000). Thus, by sensing the abundance of BIP, the unfolded protein response aims to prevent the effects described herein. It is important to note that, as with all polytopic proteins, GFP-PDS folding is coordinated from both sides of the ER membrane. Very little is known about the relationship between the cytosolic and ER-luminal folding machinery during the folding of polytopic proteins, which constitute up to 30% of the proteins in the human genome (Cobbold et al., 2003).

There is little quantitative information on the physiological levels of PDS expression in thyroid or cochlear cells, and no information on the accumulation of wild-type or mutant pendrins in intracellular organelles in Pendred syndrome patients or animal models. It is plausible to assume that the expression levels of PDS in this study are significantly higher than physiological levels, making the relevance of this work to the pathogenesis of Pendred syndrome unclear. Moreover, a recent study comparing heterologous and endogenous expression of CFTR demonstrated its efficient processing in endogenous expression systems with no requirement for ERAD. Thus, it would be interesting to study the intracellular distribution of wild-type GFP-PDS in endogenous expression systems such as thyroid follicular cells or cochlear cells, under normal physiological expression levels.

If physiological levels of PDS expression are very low (similar to GFP-PDS levels after 5-6 hours in the presence of the protein synthesis inhibitors), then the PDS should localize almost exclusively to the PM. Pendred syndrome consists of goiter and congenital deafness. The goiter is caused by a lack of function due to loss of apical iodide transport activity. However, the mechanism governing the deafness caused by PDS mutations is unknown. The potential relevance of this study to the mechanism underlying Pendred syndrome might emerge in a situation in which the accumulation of ER-retained mutant pendrins evokes a prolonged ER stress response that further induces apoptotic cell death. Such a mechanism could explain the deafness associated with Pendred syndrome. In fact, we observed that cells overexpressing GFP-L236P are extremely sensitive to ER stress induced by ALLN or tunicamycin, resulting in massive GFP-L236P aggregates (see Fig. S4 in supplementary material) and cell death.

To summarize, in this study we combined biochemical and live-cell-imaging analyses to examine the functional and morphological features of ER perturbations caused by heterologous overexpression of GFP-PDS. We found that PDS is a protein that effectively and rapidly perturbs the ER folding and degradation machineries, effects that are completely reversed by inhibition of protein biosynthesis. We put forward the idea that wild-type PDS, a misfolding-prone protein with a strong tendency to form aggregates, could be a potential tool to study cellular mechanisms of aggregate dissociation in normal and disease states.

We thank Inez Roiux and Eric D. Green (NIH) for the anti-PDS antibody, Robert Stanton (Dartmouth, NH) for the GFP-CFTR, Eric Snapp (NIH) for the YFP-SEC61β, and Sima Lev (Weizmann Institute), Edna Zolin, Ehud Gazit, Eran Barzily and Nir Osherov (Tel-Aviv University) for their critical reading of the manuscript and fruitful discussions. This work was supported in part by BSF grant 2001230, and by the V. Shreiber Medical Research Fund.

References

Bence, N. F., Sampat, R. M. and Kopito, R. R. (2001). Impairment of the ubiquitin-proteasome system by protein aggregation. *Science* **292**, 1552-1555.

Bertolotti, A., Zhang, Y., Hendershot, L. M., Harding, H. P. and Ron, D. (2000). Dynamic interaction of BiP and ER stress transducers in the unfolded-protein response. *Nat. Cell Biol.* **2**, 326-332.

Blond-Elguindi, S., Cwirla, S. E., Dower, W. J., Lipshutz, R. J., Sprang, S. R., Sambrook, J. F. and Gething, M. J. (1993). Affinity panning of a library of peptides displayed on bacteriophages reveals the binding specificity of BiP. *Cell* **75**, 717-728.

Cobbold, C., Monaco, A. P., Sivaprasadarao, A. and Ponnambalam, S. (2003). Aberrant trafficking of transmembrane proteins in human disease. *Trends Cell Biol.* **13**, 639-647.

Ellgaard, L. and Helenius, A. (2003). Quality control in the endoplasmic reticulum. *Nat Rev. Mol. Cell Biol.* **4**, 181-191.

Everett, L. A., Glaser, B., Beck, J. C., Idol, J. R., Buchs, A., Heyman, M., Adawi, F., Hazani, E., Nassir, E., Baxevanis, A. D. et al. (1997). Pendred syndrome is caused by mutations in a putative sulphate transporter gene (PDS). *Nat. Genet.* **17**, 411-422.

Gazit, E. (2002). The "correctly folded" state of proteins: is it a metastable state? *Angew Chem. Int. Ed. Engl.* **41**, 257-259.

Gillam, M. P., Sidhaye, A. R., Lee, E. J., Rutishauser, J., Waeber Stephan, C. and Kopp, P. (2004). Functional characterization of pendrin in a polarized cell system: evidence for pendrin-mediated apical iodide efflux. *J. Biol. Chem.* **279**, 13004-13010.

Goss, P. E., Baker, M. A., Carver, J. P. and Dennis, J. W. (1995). Inhibitors of carbohydrate processing: a new class of anticancer agents. *Clin. Cancer Res.* **1**, 935-944.

Hampton, R. Y. (2002). ER-associated degradation in protein quality control and cellular regulation. *Curr. Opin. Cell Biol.* **14**, 476-482.

Helenius, A. (2001). Quality control in the secretory assembly line. *Philos. Trans. R. Soc. Lond. B Biol. Sci.* **356**, 147-150.

Johnston, J. A., Ward, C. L. and Kopito, R. R. (1998). Aggresomes: a cellular response to misfolded proteins. *J. Cell Biol.* **143**, 1883-1898.

Kopito, R. R. (1999). Biosynthesis and degradation of CFTR. *Physiol. Rev.* **79**, S167-173.

Kopito, R. R. (2000). Aggresomes, inclusion bodies and protein aggregation. *Trends Cell Biol.* **10**, 524-530.

Mount, D. B. and Romero, M. F. (2004). The SLC26 gene family of multifunctional anion exchangers. *Pflugers Arch.* **447**, 710-721.

Nichols, B. J., Kenworthy, A. K., Polishchuk, R. S., Lodge, R., Roberts, T. H., Hirschberg, K., Phair, R. D. and Lippincott-Schwartz, J. (2001). Rapid cycling of lipid raft markers between the cell surface and Golgi complex. *J. Cell Biol.* **153**, 529-541.

Novoa, I., Zhang, Y., Zeng, H., Jungreis, R., Harding, H. P. and Ron, D. (2003). Stress-induced gene expression requires programmed recovery from translational repression. *EMBO J.* **22**, 1180-1187.

Presley, J. F., Cole, N. B., Schroer, T. A., Hirschberg, K., Zaal, K. J. and Lippincott-Schwartz, J. (1997). ER-to-Golgi transport visualized in living cells. *Nature* **389**, 81-85.

Rotman-Pikielny, P., Hirschberg, K., Maruvada, P., Suzuki, K., Royaux, I. E., Green, E. D., Kohn, L. D., Lippincott-Schwartz, J. and Yen, P. M. (2002). Retention of pendrin in the endoplasmic reticulum is a major mechanism for Pendred syndrome. *Hum. Mol. Genet.* **11**, 2625-2633.

Scott, D. A., Wang, R., Kreman, T. M., Sheffield, V. C. and Karniski, L. P. (1999). The Pendred syndrome gene encodes a chloride-iodide transport protein. *Nat. Genet.* **21**, 440-443.

Shefler, I. and Sagi-Eisenberg, R. (2002). Gi-mediated activation of the p42/p44 mitogen-activated protein kinases by receptor mimetic basic secretagogues is abrogated by inhibitors of endocytosis. *Int. Immunopharmacol.* **2**, 711-720.

Snapp, E. L., Hegde, R. S., Francolini, M., Lombardo, F., Colombo, S., Pedrazzini, E., Borgese, N. and Lippincott-Schwartz, J. (2003). Formation of stacked ER cisternae by low affinity protein interactions. *J. Cell Biol.* **163**, 257-269.

Taylor, J. P., Metcalfe, R. A., Watson, P. F., Weetman, A. P. and Trembath, R. C. (2002). Mutations of the PDS gene, encoding pendrin, are associated with protein mislocalization and loss of iodide efflux: implications for thyroid dysfunction in Pendred syndrome. *J. Clin. Endocrinol. Metab.* **87**, 1778-1784.

Varga, K., Jurkuvenaite, A., Wakefield, J., Hong, J. S., Guimbellot, J. S., Venglarik, C. J., Niraj, A., Mazur, M., Sorscher, E. J., Collawn, J. F. et al. (2004). Efficient intracellular processing of the endogenous cystic fibrosis transmembrane conductance regulator in epithelial cell lines. *J. Biol. Chem.* **279**, 22578-22584.

Ward, C. L. and Kopito, R. R. (1994). Intracellular turnover of cystic fibrosis transmembrane conductance regulator. Inefficient processing and rapid degradation of wild-type and mutant proteins. *J. Biol. Chem.* **269**, 25710-25718.

Ward, T. H., Polishchuk, R. S., Caplan, S., Hirschberg, K. and Lippincott-Schwartz, J. (2001). Maintenance of Golgi structure and function depends on the integrity of ER export. *J. Cell Biol.* **155**, 557-570.

Yancey, P. H., Blake, W. R. and Conley, J. (2002). Unusual organic osmolytes in deep-sea animals: adaptations to hydrostatic pressure and other perturbants. *Comp. Biochem. Physiol. A Mol. Integr. Physiol.* **133**, 667-676.

Zou, Q., Bennion, B. J., Daggett, V. and Murphy, K. P. (2002). The molecular mechanism of stabilization of proteins by TMAO and its ability to counteract the effects of urea. *J. Am. Chem. Soc.* **124**, 1192-1202.